

## Publishing Near Unity Ultraviolet Absorption in Graphene without Patterning

Jinfeng Zhu,<sup>1,4,a)</sup> Shuang Yan,<sup>1</sup> Naixing Feng,<sup>1</sup> Longfang Ye,<sup>1,b)</sup> Jun-Yu Ou<sup>2</sup> and Qing Huo Liu<sup>3</sup>

<sup>1</sup>Institute of Electromagnetics and Acoustics, and Department of Electronic Science, Xiamen University,

Xiamen, 361005, China

<sup>2</sup>Optoelectronics Research Centre and Centre for Photonic Metamaterials, University of Southampton,

Highfield, Southampton, SO17 1BJ, UK

<sup>3</sup>Department of Electrical and Computer Engineering, Duke University, Durham, NC 27708, USA

<sup>4</sup>Shenzhen Research Institute of Xiamen University, Shenzhen, 518057, China

Enhancing the light-matter interaction of graphene is an important issue for related photonic devices and applications. In view of its potential ultraviolet applications, we aim to achieve extremely high ultraviolet absorption in graphene without any nanostructure or microstructure patterning. By manipulating the polarization and angle of incident light, the ultraviolet power can be sufficiently coupled to the optical dissipation of graphene based on single-channel coherent perfect absorption in an optimized multilayered thin film structure. The ultraviolet absorbance ratios of single and four atomic layers graphene are enhanced up to 71.4% and 92.2%, respectively. Our research provides a simple and efficient scheme to trap ultraviolet light for developing promising photonic and optoelectronic devices based on graphene and potentially other 2D materials.

As the most fascinating 2D material, graphene has received great attention in photonic research from ultraviolet (UV) to terahertz ranges, and has boosted the development of advanced optics from nano-optics to angstrom-optics.<sup>1-</sup>
<sup>4</sup> In the past few years, perfect optical absorbers based on graphene have attracted a surge of research interests due to
its extraordinary electronic and photonic properties for optoelectronic devices.<sup>5,6</sup> A number of graphene-based
metamaterial absorbers in the visible, infrared and terahertz ranges have been reported for a variety of potential
applications, such as photovoltaics, photonic detection, optical modulation and thermal transfer.<sup>7-9</sup> In order to enhance
light-graphene interaction, almost all of the proposed perfect absorbers require subwavelength-scale patterning inside
or outside atomic graphene layers, and these pattern designs usually rely on technological processing in microscale or
nanoscale regimes, which will not only increase the fabrication cost dramatically, but also introduce undesirable

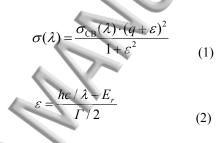
a) Email: nanoantenna@hotmail.com

b) Email: lfye@xmu.edu.cn



blishing age and contaminant to the ultrathin graphene layers in practical fabrication and degrade their ultimate electronic and photonic performance. On the other hand, in spite of these investigations, there is seldom research about the schemes to achieve extremely high UV absorption in monolayer graphene, which is also potentially promising for many applications, including UV detection, UV photoluminescence, Raman microscopy, chemical sensing, flame monitoring and space communication.<sup>10-13</sup> In this work, we are motivated to enhance UV interaction with monolayer graphene using simple and practical structure configurations without any patterning on graphene.

The thickness of monolayer graphene is much smaller than the UV wavelengths, so it can be assumed as a 2D conductive surface with a wavelength-dependent conductivity  $\sigma$ . Unlike conventional study of graphene from visible to terahertz, the many-body effects should be taken into account in the UV range.<sup>14</sup> Due to the saddle-point singularity in the electronic bands,  $\sigma$  displays a pronounced and asymmetric peak at a free space wavelength of about 268 nm, as shown in Fig. 1 (a). Under this condition,  $\sigma$  can be expressed by the following equations based on the Fano model,<sup>15</sup>



where  $\lambda$ , *h* and *c* denotes the free space wavelength, Plank constant, speed of light in vacuum, respectively;  $\varepsilon$  is the normalized energy by width  $\Gamma = 0.78$  eV relative to the resonance energy  $E_r = 5.02$  eV of the perturbed exciton;  $\sigma_{CB}(\lambda)$  is the continuum background obtained by the calculation for a many-body system, which describes the response well away from the singularity.<sup>16</sup> The Fano parameter q = -1, which determines the strength of the excitonic transition to the unperturbed band transitions and the asymmetry of the conductivity line shape. As can be seen from Fig. 1(b), the optical transmittance through a suspended graphene monolayer is higher than 91% in the UV range, and the theoretical modelling based on a finite element method (FEM) indicates good agreement with an experimental measurement from literature.<sup>17,18</sup> Based on the spectrum in Fig. 1(b), the absorbance in the UV range is higher than the visible, but the highest UV absorbance in suspended graphene is still less than 9%, which implies a pressing demand for high UV-graphene interaction efficiency for further applications.

## This manuscript was accepted by Appl. Phys. Lett. Click here to see the version of record.



**Publishing** n order to achieve extremely high UV absorption in monolayer graphene without patterning, we propose a simple and realizable methodology based on manipulating the polarization and incident angle of light on an optimized multilayered thin film structure. In our design, a metallic substrate with an optical thickness is adopted as a mirror layer to block optical transmission, and a dielectric layer with an effective subwavelength thickness is introduced to enhance UV absorption in graphene. Both the dielectric/graphene/metal (DGM) structure and graphene/dielectric/metal (GDM) structure are investigated and compared, as shown in Fig. 2(a) and Fig. 2(b). In view of the intrinsic optical absorption in various metals and material expenses as shown in Fig. 2(c), aluminum (Al) is selected as an ideal choice as the mirror layer due to its low UV loss and low cost, it has a thickness of 50 nm, and alumina (Al<sub>2</sub>O<sub>3</sub>) is used as the dielectric material.<sup>19</sup> Numerical and analytical methods are adopted to optimize and enhance UV absorption of graphene for the following discussions.

We first consider the general effects of DGM and GDM structures on UV absorption enhancement of graphene with polarization and angle manipulation of incident light. Normal and oblique incidences for both p- and s-polarized lights are investigated, as shown in Fig. 3. Particularly, a continuous ultrathin hexagonal boron nitride (hBN) layer of 1 nm is used to isolate graphene from aluminum electron doping for the DGM structure, which is different from the boron nitride doping in graphene.<sup>20</sup> In this case, the graphene monolayers for both GDM and DGM structures have comparable optical conductivities for equitable comparison and further discussion. The hBN is assumed to be optically lossless,<sup>21</sup> because its band gap is wide enough and beyond the discussed UV wavelength range larger than 240nm.<sup>22-</sup> <sup>24</sup> In the UV range, graphene acts as a lossy conductive surface, and it is infeasible to excite plasmon polaritons by *p*polarized light and induce strong UV-graphene interaction like that in the terahertz and infrared range, where only the intra-band transition dominates the optical response.<sup>25</sup> As shown in Fig. 3(a) and Fig. 3(b), the optical absorbance under *p*-polarized light for both structures does not show remarkable enhancement, the UV absorbance for the DGM structure is even lower than the suspended graphene, and the UV absorbance for the GDM structure under normal incidence is slightly enhanced with a broad absorption band extended to the visible range. In contrast, the optical absorbance in Fig. 3(c) and Fig. 3(d) under s-polarized light for both structures indicates predominant narrow-band UV absorption enhancement with extremely-suppressed visible absorbance (almost zero), especially under the oblique incidence of 85°. Besides, Fig. 3(c) and Fig. 3(d) demonstrate that the optical absorbance evolves from a broad band to a narrow band with a dominant peak at  $\lambda = 314$  nm in the UV range, as the incident angle increases from 0° to 85°, and the GDM structure shows an overwhelming advantage of UV absorbance enhancement up to 63.1% versus the



Publishing: I structure with an absorbance of only 18.2%. The enhancement for the UV absorbance peak of graphene for both structures can be attributed to coherent perfect absorption for the one-port UV network,<sup>26,27</sup> in which the polarized light enters a multilayered structure of ultrathin films with a metal mirror through a single channel using a critical coupling angle. The perfect absorption originates from destructive self-interference and dissipation in the lossy material layers, including graphene and aluminum. The GDM structure is much more advantageous than the DGM structure, because it has more light absorption contributed to graphene instead of aluminum based on the absorbance calculation for different materials.

We next analyze why *s*-polarized light has much better absorption enhancement than *p*-polarized light, as shown in Fig. 3. Graphene can be assumed as a non-magnetic (*i.e.* permeability  $\mu = \mu_0$ ) 2D material with in-plane isotropy, and the optical loss in graphene is induced by its conductive 2D surface with in-plane Ohmic dissipation, so the optical absorption is only determined by the electric field component parallel to the graphene surface. The electric field of an *s*-polarized light is always parallel to the graphene surface, and this provides an essential condition to significantly enhance the absorption of graphene under the critical coupling condition for a certain oblique incident angle; whereas the electric field of a *p*-polarized light for various incident angles is not always parallel to the graphene surface and only the parallel component of electric field contributes to the optical loss of graphene, so the optical loss in graphene is gradually reduced as the incident angle becomes larger and larger. As can be observed in Fig. 4 for the full-wave FEM simulation of a GDM structure, compared with the *p*-polarized light, the *s*-polarized light has much higher inplane field intensities surrounding the graphene layer at  $\lambda = 314$  nm, which gives rise to enhanced surface current densities on the single layer crystal of hexagonal carbon atoms, and leads to much stronger light-graphene interaction and much more UV absorption in graphene. Since *p*-polarized light is infeasible for high absorbance in graphene and the GDM structure demonstrates considerable potential for absorption enhancement, we focus on investigations with *s*-polarized light for the GDM structure in the following discussions.

We further reveal the physics insight by an analytical method. For the one-port UV network, the scattering-matrix equation can be simplified as  $b_1 = ra_1$ , where *r* is the total reflection coefficient of the GDM structure,  $a_1$  and  $b_1$  are the complex scalars for the input and output wave amplitudes, respectively. Based on the Fresnel-Airy formalism,<sup>28</sup> *r* can be expressed as below



$$r = \frac{r_{12} + r_{2-4}e^{2i\beta_2}}{1 + r_{12}r_{2-4}e^{2i\beta_2}}$$
(3)

$$r_{2-4} = \frac{r_{23} + r_{34}e^{2i\beta_3}}{1 + r_{23}r_{34}e^{2i\beta_3}}$$
(4)

Here,  $r_{ij}$  represents the Fresnel coefficient from medium *i* to medium *j* as shown in Fig. 3(d),  $\beta_i = 2\pi N_i d_i \cos\theta_i / \lambda$  is the phase factor in medium *i*, and  $N_i$ ,  $d_i$  and  $\theta_i$  are the complex refractive index, thickness and light angle for medium *i*. The effective complex refractive index of graphene can be represented by its surface conductivity.<sup>29</sup> Based on Snell's law, we define  $\theta_i = \arcsin(N_1 \sin\theta_1 / N_i)$ , which can be complex-valued and denote loss in medium *i*. The field Fresnel reflection coefficient  $r_{ij}$  for *s*-polarized light from medium *i* to medium *j* can be expressed as below

$$r_{ij} = \frac{N_i \cos \theta_i - N_j \cos \theta_j}{N_i \cos \theta_i + N_j \cos \theta_j}$$
(5)

The optical skin depth of aluminum is  $\delta(\lambda) = \lambda/[2\pi k(\lambda)]$ , where  $k(\lambda)$  is the imaginary part of the wavelengthdependent complex refractive index of aluminum, and it is less than 15.1 nm in the discussed spectral range. Hence, the thickness of 50 nm aluminum layer is large enough to block the transmittance T(i.e. T=0), and the total absorbance in the structure is  $A = A_G + A_{AI} = 1 - R$ , where R is the total reflectance, and  $A_G$  and  $A_{AI}$  denote the fractions of absorbance in graphene and aluminum, respectively.  $A_G$  and  $A_{AI}$  becomes larger simultaneously, as the coherent perfect absorption is gradually approached by changing the incident angle. In order to reach the maximum absorbance of graphene,  $R = |r|^2$  should equal to zero. According to equation (3) and (4), we can obtain the equation  $r_{23}+r_{34}\cdot e^{2i\beta_2} =$ 0, if graphene is lossless. This implies a self-interference mode, which can be related to a resonance condition corresponding to a situation where the complete round-trip phase accumulation inside the structure is  $2\pi$ . The coherent perfect absorption can be achieved with a UV resonance for A = 1 at a critical angle.

The total absorbance of the GDM structure as a function of incident angle and wavelength is further calculated by an analytical method using characteristic matrices for thin films.<sup>28</sup> The analytical result in Fig. 5(a) indicates perfect consistency with the FEM simulation result in Fig. 5(b), and these results show that the GDM structure completely absorbed the light in the UV range, when the critical coupling angle is 84.1° and the wavelength is 313 nm. For the angle range from 80.7° to 86.2°, the total absorbance in the UV range is extremely high (larger than 95%), and the



Publishing bance is originated from the loss in both graphene and aluminum. Although the light power is partially dissipated in aluminum, most of the light power is absorbed by graphene under the critical coupling angle, as shown in Fig. 5 (c). For an alumina layer of 40 nm, graphene absorbs up to 63.5% of UV light at the wavelength of about 314 nm under the incidence of 84.2°, which is basically consistent with the critical coupling angle for absolute absorption of the GDM structure, and graphene maintains the absorbance ratios of over 50% for incident angles from 74.5° to 87.8°. Based on above analysis for Fig. 5(a) ~ Fig. 5(c), we can generally optimize the critical coupling parameters for coherent perfect absorption of a GDM structure in order to reach the maximum absorption in graphene. Fig. 5(a) ~ Fig. 5(c) also demonstrate that a critical angle determines the maximum total absorbance at a certain central wavelength for a given thickness of alumina. Therefore, in Fig. 5(d), we illuminate the critical angle coupling conditions for maximum absorbances at various central wavelengths by tuning the thickness of alumina layer within the subwavelength limit. Fig. 5(d) indicates good agreement between the analytical model and FEM simulation, and demonstrate the optimization mechanism of maximum absorbance for different UV central wavelengths in combination with distinct critical angles.

Finally, we investigate the effects of the alumina thickness and the atomic layer number in graphene, because the UV central wavelengths and incident angles are also tightly related with these two factors. As shown in Fig. 6(a), when we change the thickness of alumina from 10 nm to 100 nm under 85° incidence of *s*-polarized light, the absorption band has a red shift from the UV range to the visible range. As the thickness of alumina increases from 27 nm to 55 nm, the absorption peak position varies from 240 nm to 400 nm. The peak shift is attributed to the change of phase factor in the alumina layer, as demonstrated in the above analytical method for coherent perfect absorption. Based on the expression of phase factor  $\beta_i = 2\pi N_i d_i \cos \theta_i / \lambda$ , the wavelength of absorption peak should be changed proportionally to the thickness of alumina, in order to maintain the minimum reflection derived from equation (3) , (4) and (5). Thus, one can tune the thickness of the alumina thin film for a GDM structure in order to confine the light trapping on graphene in the UV range. Based on the discussion about the dielectric thickness, we optimize the absorbance of graphene with various numbers of atomic layer, and each maximum has been achieved at  $\lambda = 268$  nm under the corresponding thickness of alumina and incident angle, as observed in Fig. 6(b). The maximum absorbance raises from 71.4% to 92.2% in the UV range, as the number of graphene atomic layer gradually raises from 1 to 4. This is because the optical conductivity of graphene becomes larger as the number of atomic layer increases,<sup>15</sup> which leads to more UV dissipation in graphene. The monolayer graphene has a narrower UV absorption band with high

## This manuscript was accepted by Appl. Phys. Lett. Click here to see the version of record.

Publishing ression of visible absorption, while the 4-layer graphene possesses a broader band with higher absorbance, partially extended to the visible range. With the optimized alumina thickness and coupling angle, larger conductivity of graphene induces lower loss in aluminum and higher optical absorption in graphene with a broader band.

In summary, we propose to a simple thin-film structure for extremely high UV absorption in graphene without patterning by single-channel coherent perfect absorption. The work provides an efficient method to trap UV light in graphene for developing high-performance UV devices.

This work was supported by China Scholarship Council, Shenzhen Science and Technology Innovation Committee (JCYJ20170306141755150) and Fujian Provincial Department of Science and Technology (2017J01123).

- <sup>1</sup> F. J. García de Abajo, "Graphene nanophotonics," Science **339**, 917-918 (2013).
- <sup>2</sup> Q. Ding, Y. Shi, M. Chen, H. Li, X. Yang, Y. Qu, W. Liang and M. Sun, "Ultrafast dynamics of plasmon-exciton interaction of Ag nanowire-graphene hybrids for surface catalytic reactions," Sci. Rep. 6, 32724 (2016).
- <sup>3</sup> D. N. Basov, M. M. Fogler and F. J. García de Abajo, "Polaritons in van der Waals materials," Science 354, aag1992 (2016)
- <sup>4</sup> E. Cao, X. Guo, L. Zhang, Y. Shi, W. Lin, X. Liu, Y. Fang, L. Zhou, Y. Sun, Y. Song, W. Liang and M. Sun, "Electrooptical Synergy on Plasmon–Exciton-Codriven Surface Reduction Reactions," Adv. Mater. Interfaces, 4, 1700869 (2017).
- <sup>5</sup> S. Thongrattanasiri, F. H. Koppens and F. J. G. De Abajo, "Complete optical absorption in periodically patterned graphene," Rev. Lett. **108**, 047401 (2012).
- <sup>6</sup> J. R. Piper and S. Fan, "Total absorption in a graphene monolayer in the optical regime by critical coupling with a photonic crystal guided resonance," ACS Photonics 1, 347-353 (2014).
- <sup>7</sup> Y. Cai, J. Zhu and Q. H. Liu, "Tunable enhanced optical absorption of graphene using plasmonic perfect absorbers," Appl. Phys. Lett. **106**, 043105 (2015).
- <sup>8</sup> Z. Sun, A. Martinez and F. Wang, "Optical modulators with 2D layered materials," Nat. Photonics 10, 227-238 (2016).
- <sup>9</sup> Z. Su, J. Yin and X. Zhao, "Terahertz dual-band metamaterial absorber based on graphene/MgF<sub>2</sub> multilayer structures," Opt. Express **23**, 1679-1690 (2015).
- <sup>10</sup> J. Li, L. Niu, Z. Zheng and F. Yan, "Photosensitive graphene transistors," Adv. Mater. 26, 5239-5273 (2014).
- <sup>11</sup> V. Q. Dang, T. Q. Trung, D. I. Kim, L. T. Duy, B. U. Hwang, D. W. Lee, B. Y. Kim, L. D. Toan and N. E. Lee, "Ultrahigh responsivity in graphene-ZnO nanorod hybrid UV photodetector," Small **11**, 3054-3065 (2015).
- <sup>12</sup> L. Tang, R. Ji, X. Cao, J. Lin, H. Jiang, X. Li, K. S. Teng, C. M. Luk, S. Zeng, J. Hao and S. P. Lau, "Deep ultraviolet photoluminescence of water-soluble self-passivated graphene quantum dots," ACS nano. 6, 5102-5110 (2012).
- <sup>13</sup> H. L. Liu, S. Siregar, E. H.vHasdeo, Y. Kumamoto, C. C. Shen, C. C. Cheng, L. J. Li, R. Saito and S. Kawata, "Deepultraviolet Raman scattering studies of monolayer graphene thin films," Carbon 81, 807-813 (2015).
- K. F. Mak, L. Ju, F. Wang and T. F. Heinz, "Optical spectroscopy of graphene: from the far infrared to the ultraviolet," Solid State Commun. **152**, 1341-1349 (2012).



- Publishingk. F. Mak, J. Shan and T. F. Heinz, "Seeing many-body effects in single-and few-layer graphene: observation of twodimensional saddle-point excitons," Phys. Rev. Lett. **106**, 046401 (2011).
  - <sup>16</sup> L. Yang, J. Deslippe, C. H. Park, M. L. Cohen and S. G. Louie, "Excitonic effects on the optical response of graphene and bilayer graphene," Phys. Rev. Lett. **103**, 186802 (2009).
  - <sup>17</sup> S. Bae, H. Kim, Y. Lee, X. Xu, J. S. Park, Y. Zheng, J. Balakrishnan, T. Lei, H. R. Kim, Y. I. Song, Y. J. Kim, K. S. Kim, B. Özyilmaz, J. H. Ahn, B. H. Hong and S. Lijima, "Roll-to-roll production of 30-inch graphene films for transparent electrodes," Nat. Nanotechnol. 5, 574-578 (2010).
  - <sup>18</sup> J. Niu, M. Luo, J. Zhu and Q. H. Liu, "Enhanced plasmonic light absorption engineering of graphene: simulation by boundary-integral spectral element method," Opt. Express 23, 4539-4551 (2015).
  - <sup>19</sup> E. D. Palik, Handbook of Optical Constants of Solids 3 (Academic Press, 1998).
  - <sup>20</sup> C.-K. Chang, S. Kataria, C.-C. Kuo, A. Ganguly, B.-Y. Wang, J.-Y. Hwang, K.-J. Huang, W.-H. Yang, S.-B. Wang, C.-H. Chuang, M. Chen, C.-I Huang, W.-F. Pong, K.-J. Song, S.-J. Chang, J.-H. Guo, Y. Tai, M. Tsujimoto, S. Isoda, C.-W. Chen, L.-C. Chen and K.-H. Chen, "Band gap engineering of chemical vapor deposited graphene by in situ BN doping", ACS Nano, 7, 1333-1341, 2013
  - <sup>21</sup> T. Ishii and T. Sato, "Growth of single crystals of hexagonal boron nitride," J. Cryst. Growth 61, 689-690 (1983).
  - <sup>22</sup> J. Wang, F. Ma, W. Liang, R. Wang and M. Sun, "Optical, photonic and optoelectronic properties of graphene, h-NB and their hybrid materials," Nanophotonics 6, 943–976 (2017).
  - <sup>23</sup> J. Wang, F. Ma, W. Liang and M. Sun, "Electrical properties and applications of graphene, hexagonal boron nitride (h-BN), and graphene/h-BN heterostructures," Mater. Today Phys. 2, 6-34 (2017).
  - <sup>24</sup> J. Wang, X. Xu, X. Mu, F. Ma and M. Sun, "Magnetics and spintronics on two-dimensional composite materials of graphene/hexagonal boron nitride," Mater. Today Phys. **3**, 97-117 (2017).
  - <sup>25</sup> T. Low, A. Chaves, J. D. Caldwell, A. Kumar, N. X. Fang, P. Avouris, T. F. Heinz, F. Guinea, L. M. Moreno and F. Koppens, "Polaritons in layered two-dimensional materials," Nat. Mater. 16, 182-194 (2017).
  - <sup>26</sup> D. G. Baranov, A. Krasnok, T. Shegai, A. Alù and Y. Chong, "Coherent perfect absorbers: linear control of light with light," Nat. Rev. Mater. 2, 17064 (2017).
  - <sup>27</sup> J. Linder and K. Halterman, "Graphene-based extremely wide-angle tunable metamaterial absorber," Sci. Rep. 6, 31225 (2016).
  - <sup>28</sup> H. A. Macleod, Thin-Film Optical Filters, (CRC Press, Boca Raton, 2010).
  - <sup>29</sup> Y. Cai, J. Zhu, Q. H. Liu, T. Lin, J. Zhou, L. Ye and Z. Cai, "Enhanced spatial near-infrared modulation of graphene-loaded perfect absorbers using plasmonic nanoslits," Opt. Express 23, 32318-32328 (2015).

**FIG. 1.** (a) Optical conductivity  $\sigma$  of graphene as a function of free space wavelength  $\lambda$ . Inset is the band structure of graphene with the saddle point singularity at the M point. (b) Experimental and theoretical results of optical transmittance through monolayer graphene.

FIG. 2. Schematic drawings for (a) DGM structure and (b) GDM structure and (c) optical absorbance of various metals under normal incidence

**FIG. 3.** Optical absorbance ratios of graphene for both structures under various polarizations and incident angles  $\theta$  based on the FEM modelling: (a) *p*-polarized light on the DGM structure, (b) *p*-polarized light on the GDM structure,



Publishings-polarized light on the DGM structure, and (d) *s*-polarized light on the GDM structure. All the thicknesses of alumina are fixed at 40 nm.

**FIG. 4.** Electric field distributions on the GDM structure for *p*- and *s*-polarized light under 85° incidence, where  $|E_p|$  denotes the amplitude of the electric field component parallel to the graphene surface.

**FIG. 5.** (a) Analytical modelling and (b) FEM simulation for total absorbance of the GDM structure, and (c) simulated absorbance of graphene for the GDM structure, as functions of free space wavelength and incident angle for *s*-polarized light and an alumina layer of 40 nm. (d) Critical angles for maximum absorbance at various central wavelengths with optimized alumina thicknesses.

FIG. 6. (a) Absorbance of monolayer graphene as a function of wavelength and alumina thickness, where the incident angle of *s*-polarized light is 85° on a GDM structure. (b) Optimized absorbance ratios of graphene with the maximum at  $\lambda = 268$  nm, in which various atomic layers correspond to relevant alumina thicknesses *d* and critical coupling angles  $\theta$ .

